Molecular Therapy
Nucleic Acids
Original Article

Exosomal miRNA-320a Is Released from hAMSCs and Regulates SIRT4 to Prevent Reactive Oxygen Species Generation in POI

Chenyue Ding,[1,4] Chunfeng Qian,[1,2,4] Shunyu Hou,[3,4] Jiafeng Lu,[1] Qinyan Zou,[1] Hong Li,[1,2] and Boxian Huang[1,2]

[1]Center of Reproduction and Genetics, Affiliated Suzhou Hospital of Nanjing Medical University, Suzhou Municipal Hospital, Suzhou, 215002, China; [2]State Key Laboratory of Reproductive Medicine, Nanjing Medical University, Nanjing 210029, China; [3]Department of Obstetrics and Gynecology, Affiliated Suzhou Hospital of Nanjing Medical University, Suzhou Municipal Hospital, Suzhou 215002, China

Human amniotic mesenchymal stem cells (hAMSCs) were previously shown to effectively rescue ovarian function in a premature ovarian insufficiency (POI) mouse model. The therapeutic mechanism of hAMSC-derived exosomes (hAMSC-Exos) is not fully understood. In this study, the therapeutic mechanism involved in exosomal microRNA-320a (miR-320a) and Sirtuin 4 (SIRT4) was investigated in POI mouse ovaries oocytes and human granulosa cells (hGCs) by fluorescence-activated cell sorting (FACS), hematoxylin and eosin (H&E) staining, enzyme-linked immunosorbent assay (ELISA), and immunofluorescence experiments. hAMSC-Exos improved proliferation, inhibited apoptosis, and decreased the expression of SIRT4 and relative genes in POI hGCs and ovaries. hAMSC-Exos elevated ovarian function and prohibited SIRT4 expression in oogenesis. The therapeutic effects were attenuated when miR-320a was knocked down. hAMSC-Exos decreased the ROS levels in POI hGCs and oocytes and improved ovarian weight and litter size, except for the Exos$^{anti\text{-}miR\text{-}320a}$/POI group. Finally, hAMSC-Exos reduced the SIRT4 and ROS levels in POI ovaries and hGCs. The downstream protein expression (ANT2, AMP-dependent kinase [AMPK], and L-OPA1) was downregulated in the hGCs-SIRT4^{KD} group but disappeared in the Exos$^{anti\text{-}miR\text{-}320a}$/POI group. Our study is the first to illustrate the therapeutic potential of hAMSC-Exos in POI. Exosomal miR-320 plays a key role in the hAMSC-Exos-mediated effects on ovarian function via SIRT4 signaling.

INTRODUCTION

Premature ovarian insufficiency (POI) is one of the most common clinical syndromes, defined as loss of physiological integrity and organ function associated with amenorrhea before the age of 40; the major causes are mitochondrial dysfunction, chemotherapeutic treatments, and cellular senescence.[1] Currently, it is difficult to restore ovarian function with sequential hormone replacement therapy, which is accompanied by side effects.[2] With the development of regenerative medicine, mesenchymal stem cells (MSCs) possess characteristics such as differentiation potential into tridermic, self-renewing tissues without teratoma formation, which makes them a cellular source for tissue damage repair and the treatment of many diseases in organ systems.[3] Numerous studies have shown that MSCs derived from many tissues inhibit oocyte decay, enhance oogenesis, and promote fertility; these MSCs include human amniotic mesenchymal stem cells (hAMSCs), human adipose-derived stem cells (hADSCs), and human bone marrow-derived mesenchymal stem cells (hBMSCs).[4–6] Nevertheless, little is known about the rigorous molecular mechanism of hAMSC-based therapies in premature-associated damage to ovarian function.

Exosomes are small vesicles with a size of 30–150 nm that are released from MSCs and can mediate cell-to-cell communication by carrying various biomolecules, including mRNAs, microRNAs (miRNA), long non-coding RNAs (lncRNAs), and proteins.[7,8] These nanoparticles have regenerative effects in experimental models of tissue repair injury and aging.[9] Growing evidence has shown that exosomes derived from human umbilical cord MSCs inhibit apoptosis in mouse ovarian granulosa cells.[10] Human umbilical cord blood-derived exosomal miR-21-3p triggered re-epithelialization in wound healing.[11] However, whether MSCs recover reproductive function and promote gametogenesis by transferring exosomal miRNAs and the relative mechanism is not entirely understood.

Oxidative stress is mostly generated in mitochondria during aging.[12] Reproductive capacity is very sensitive to the redox balance, antioxidant enzyme, and oxidant enzyme levels.[13] Abnormal generation of oxidative stress/reactive oxygen species (ROS) can disturb the process of biological development, such as oxidative damage in DNA and

Received 8 March 2020; accepted 14 May 2020;
https://doi.org/10.1016/j.omtn.2020.05.013.

[4]These authors contributed equally to this work.

Correspondence: Boxian Huang, Center of Reproduction and Genetics, Affiliated Suzhou Hospital of Nanjing Medical University, Suzhou Municipal Hospital, Suzhou 215002, China.
E-mail: huangboxiannj@163.com
Correspondence: Hong Li, Center of Reproduction and Genetics, Affiliated Suzhou Hospital of Nanjing Medical University, Suzhou Municipal Hospital, Suzhou 215002, China.
E-mail: hongliszivf@163.com

cellular senescence.[13] In line with reproductive aging, ROS levels were observably increased in ovaries and oocytes.[14] Besides, oxidative damage accelerated the mouse ovarian aging by decreasing the expression of antioxidant genes.[15] Previous studies indicated that cyclophosphamide (CTX) induced high-level oxidative stress, which increased apoptosis in human granulosa cells (hGCs).[16]. Sirtuins have been shown to play a critical role in the regulation of key processes in lifespan, aging, and metabolism.[17] There are seven enzymes (SIRTs 1–7) in the sirtuin family that have also been linked to regulate various biological functions.[17] Therefore, SIRT4 is critical for cellular metabolism and DNA damage responses.[18] SIRT4 can take part in the maintenance of cellular and organismal physiology function in mitochondria.[19] A recent study indicated that SIRT4 overexpression induced cell aging. A previous study also revealed that SIRT4 upregulation can induce accelerated aging in oocytes.[20] AMP-dependent kinase (AMPK), adenine nucleotide translocator 2 (ANT2), and GTPase optic atrophy type 1 (OPA1) are central sensors of cellular energy status and mitochondrial dynamics.[21] Previous reports showed that ANT2 could be a latent substrate of SIRT4.[21] In addition, SIRT4 has the ability to regulate mitochondrial ATP homeostasis via crosstalk between ANT2 and AMP. The SIRT4-OPA1 axis is related directly to age-associated decreased mitophagy by promoting mitochondrial fusion.[22]

In the present study, exosomes were obtained from hAMSCs and explored the antiaging potential of hAMSC-Exos in ovaries, hGCs, and oocytes. We found that hAMSC-Exos promoted proliferation, inhibited ROS levels, and downregulated SIRT4 and related gene expression levels in *in vivo* and *in vitro* models. We analyzed the miRNA profiles of hAMSC-Exos and found that miR-320a-3p was enriched in hAMSC-Exos. After miR-320a knockdown in hAMSCs, the effects of stem cell therapy disappeared in the process of oogenesis. It is the first to show the ability of hAMSC-Exos to restore ovarian aging. Furthermore, in the current study, the detailed underlying mechanisms have been revealed where hAMSC-derived exosomal miR-320a results in premature resistance in ovaries and oocytes by targeting SIRT4.

RESULTS

Isolation and Identification of hAMSCs and Related Exosomes

With the goal of evaluating the character of purified nanoparticles derived from hAMSCs, transmission electron microscopy (TEM), western blotting, and the fluorescence-activated cell sorting (FACS) method were employed in this detection. TEM experiments revealed that the hAMSC-Exos were 30–150 nm spheres and exhibited a cobblestone-like morphology with a complete membrane structure in Figure S1A. Further characterization of hAMSC-Exos by western blot (WB) analysis confirmed that the exosomal surface markers Alix, TSG101, CD9, CD63, and CD81 were positively expressed, while few expressed the marker CD105 (Figure S1B). According to the FACS assay results, hAMSC-Exos were significantly expressed exosome markers CD63, CD9, and CD81 (Figure S1C). Besides, our results indicated that hAMSC-Exos were confirmed as mean diameters of 144.6 nm (Figure S1D). All of these data demonstrated the successful harvest of hAMSC-Exos from the culture medium for future therapeutic experiments.

hAMSC-Exos Inhibited Apoptosis, Improved Proliferation, and Affected SIRT4 and Downstream Gene Expression in hGCs

To explore the therapeutic effect of hAMSC-Exos on cell proliferation and apoptosis in POI hGCs, we first used a FACS assay to detect the proliferation rate of hGCs after coculture with hAMSC-Exos. The data showed that the proliferation levels of POI hGCs were enhanced in a dose-dependent manner (Figure 1A). In addition, with the high concentration of Exos (10×10^{10} particles/mL), the cell death rate was inhibited significantly in a time-dependent manner (Figure 1B). The protein results revealed that the anti-apoptosis genes (SURVIVIN and BCL2) were activated by hAMSC-Exos in a dose-dependent manner (Figures 1C and 1D); the apoptosis genes (CASPASE3 and CASPASE9) were also prohibited more effectively after treatment with hAMSC-Exos, as the concentration of Exos increased (Figures 1E and 1F). We assessed the gene and protein expression levels of SIRT4 and its relative genes ANT2, AMPK, and L-OPA1 in POI hGCs after treatment with four concentrations of exosomes. Our experimental results indicated that the expression level of SIRT4 was decreased to a normal level in a dose-dependent manner with exosome concentrations ranging from 0 to 10×10^{10} particles/mL (Figure 1G). The gene and protein assays also demonstrated that the expression of downstream genes (ANT2, AMPK, and L-OPA1) was reduced gradually with concentration-dependent exosomes (Figures 1H–1K).

In brief, these results suggested that hAMSC-Exos could improve activity and inhibit the oxidative stress regulator SIRT4 in POI hGCs.

hAMSC-Exos Reduced Apoptosis, Elevated Proliferation, and Decreased SIRT4 and Downstream Gene Expression in POI Mouse Ovaries

To evaluate the role of hAMSC-Exos on the protection of ovarian function in the POI mouse model, we injected CM-Dil-labeled Exos with different concentrations (0 to 100×10^{10} particles/mL) directly into the ovary. 4 weeks later, hAMSC-Exos appeared in the ovary and surrounding oocyte (Figure 2A). In addition, an immunofluorescence experiment was carried out to assess the ability of proliferation in POI ovaries with four concentrations of Exos. As shown in Figure 2B, the CTX-induced decrease in bromodeoxyuridine (BrdU) expression in the ovary could be reversed observably by an increase in the injected concentration of Exos, especially up to 100×10^{10} particles/mL. The survival rate was also evaluated in the highest concentration group of Exos. Our results showed that the survival rate remained stable and higher in the treatment group than in the POI group without treatment (Figure 2C). Furthermore, we found that the protein levels of anti-apoptosis genes were increased (Figures 2D and 2E) and apoptosis genes were repressed after hAMSC-Exos injection (Figures 2F and 2G). Afterward, we detected the expression of proteins relative to SIRT4 following treatment with hAMSC-Exos. The expression of SIRT4 was obviously suppressed in POI ovaries by hAMSC-Exos in a dose-dependent manner, as analyzed using western blotting (Figure 2H). Downstream genes were also analyzed at the mRNA and

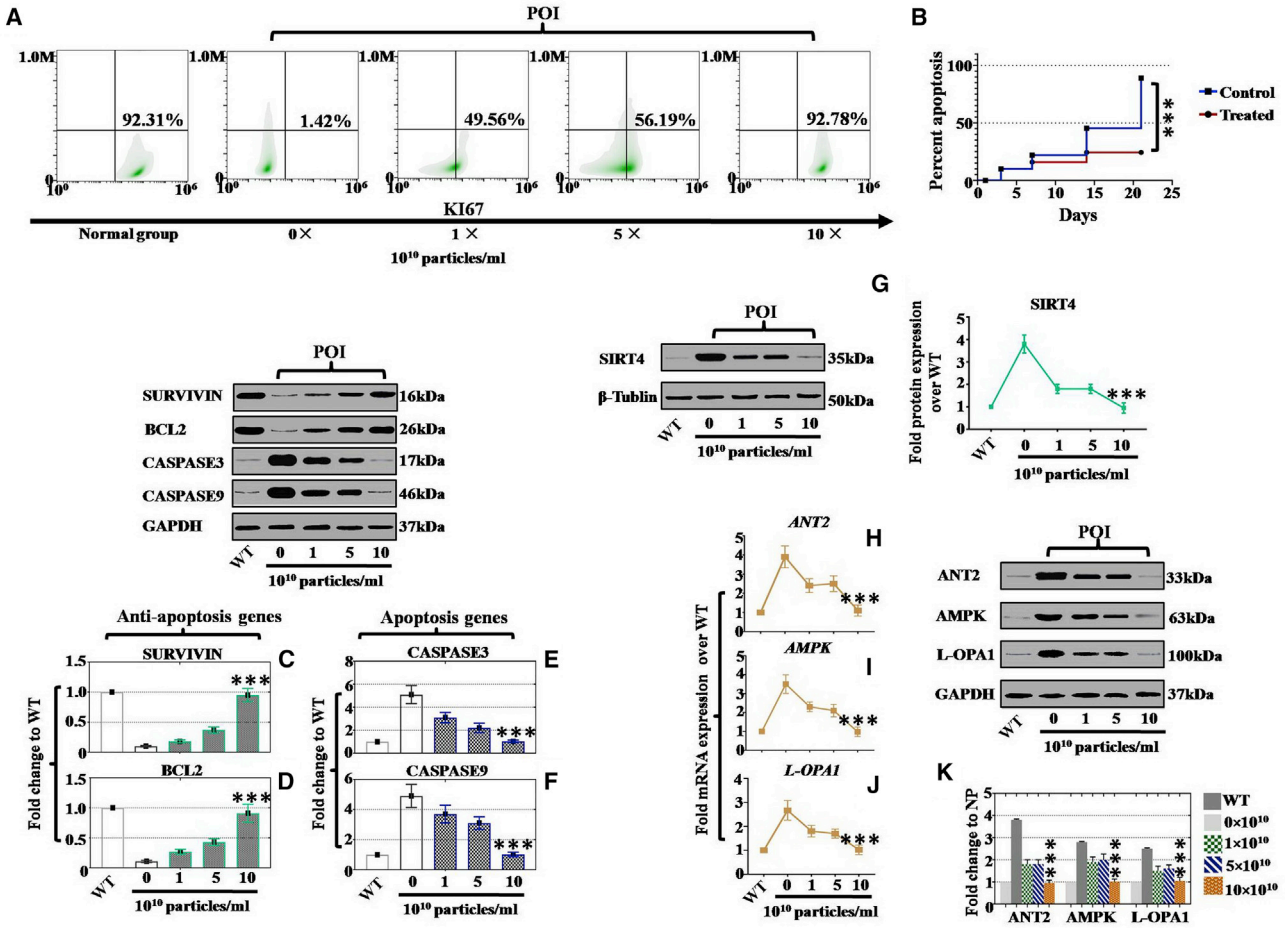

Figure 1. hAMSC-Exos Inhibited Apoptosis and SIRT4 Expression in CTX-Damaged hGCs

(A) FACS scatterplots showing that hAMSC-Exos increased the percentage of KI67$^+$ cells in CTX-damaged hGCs in a dose-dependent manner. (B) The apoptosis curves of the POI hGCs after hAMSC-Exos were co-cultured. (C) WB results illustrating that hAMSC-Exos improved SURVIVN expression in CTX-damaged hGCs in a dose-dependent manner. (D) WB results illustrating that hAMSC-Exos elevated BCL2 expression in CTX-damaged hGCs in a dose-dependent manner. (E) WB results indicating that hAMSC-Exos inhibited CASPASE3 expression in CTX-damaged hGCs in a dose-dependent manner. (F) WB results indicating that hAMSC-Exos prohibited CASPASE9 expression in CTX-damaged hGCs in a dose-dependent manner. (G) Protein-level analysis indicating that hAMSC-Exos suppressed the SIRT4 expression in CTX-damaged hGCs with a dose-dependent manner. (H–J) mRNA-level analysis showing that hAMSC-Exos increased relative gene (ANT2, AMPK, and L-OPA1) expression in CTX-damaged hGCs in a dose-dependent manner. (K) Protein-level analysis showing that hAMSC-Exos decreased apoptosis genes (ANT2, AMPK, and L-OPA1) expression in CTX-damaged hGCs in a dose-dependent manner. All experiments were repeated three times. Error bars indicate SD. ***$p < 0.001$.

protein levels. As shown in Figures 2I–2K, Exos significantly decreased the mRNA levels of ANT2, AMPK, and L-OPA1, which were more powerful and correlated to increased concentrations of Exos. The WB data revealed similar results (Figure 2L).

In short, the above results revealed that injection of hAMSC-Exos elevated ovarian vitality and repressed oxidative stress genes dose-dependently.

hAMSC-Exos Contain miR-320a Predicted to Regulate a Tissue-Regenerative Target SIRT4

miRNAs are another type of key molecule in exosomes. To explore the mechanism of hAMSC-Exos in rescuing POI mice, we used miRNA microarrays to measure the expression levels of various miRNAs in hAMSC-Exos. HDF-derived Exos act as a control group. From the heatmap, miRNAs in hAMSC-Exos were profiled by rank ordered according to the total reads. Compared to the HDF-Exos group, the hAMSC-Exos group had an enriched degree of the top 6 miRNAs, which from highest to lowest were: miR-320a, miR-146a, miR125b, miR-335, miR-199a, and miR-127 (Figure 3A). After executing a Kyoto encyclopedia of genes and genomes (KEGG) signal pathway analysis of the top 6 miRNA sequencing results in activated pathways and biological processes, the network of miRNAs was predicted to target that was mainly enriched in the PI3K-AKT and Notch pathways (Figure 3B). The results of the quantitative reverse transcriptase polymerase

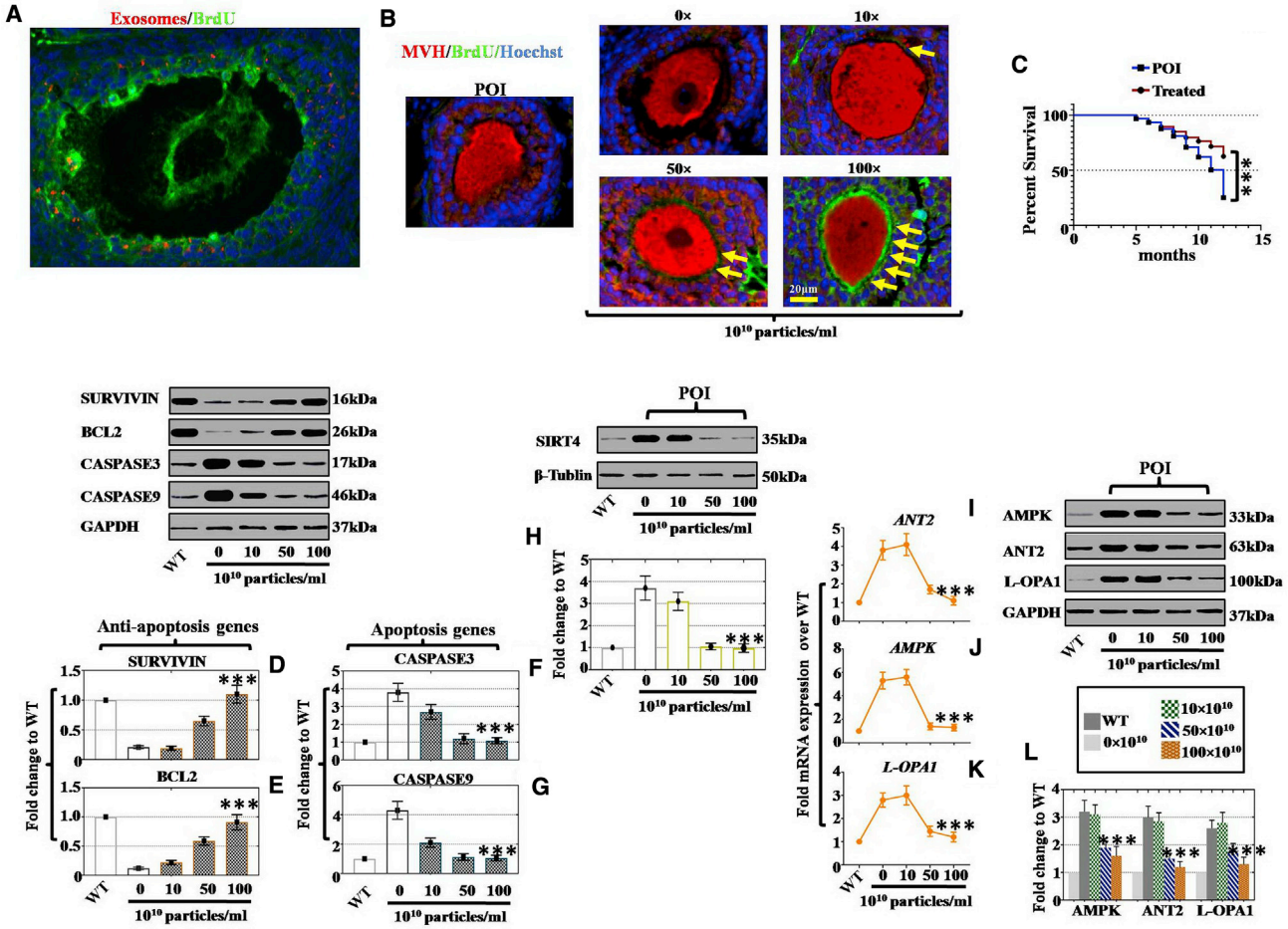

Figure 2. hAMSC-Exos Improved Proliferation and SIRT4 in POI Mice Model

(A) Fluorescence microscopy image of the mouse ovarian section showing the transplanted CM-DiI-labeled (red) hAMSC-Exos and the expression of BrdU (green). Scale bar, 20 μm. (B) Fluorescence microscopy view of the mouse ovarian sections showing that hAMSC-Exos transplantation increased proliferation level in a dosage-dependent by staining with BrdU (green). Scale bar, 20 μm. (C) The survival curves of the POI mouse after hAMSC-Exos therapy. Sham, n = 10; the treatment groups, n = 10. (D) Protein-level analysis indicating that hAMSC-Exos transplantation increased SURVIVIN expression in CTX-induced POI mice model in a dosage-dependent manner. (E) Protein-level analysis indicating that hAMSC-Exos transplantation increased BCL2 expression in CTX-induced POI mice model in a dosage-dependent manner. (F) Protein-level analysis indicating that hAMSC-Exos transplantation decreased CASPASE3 expression in CTX-induced POI mice model in a dosage-dependent manner. (G) Protein-level analysis indicating that hAMSC-Exos transplantation inhibited CASPASE9 expression in CTX-induced POI mice model in a dosage-dependent manner. (H) WB results illustrating that hAMSC-Exos transplantation suppressed SIRT4 expression in CTX-induced POI mice model in a dosage-dependent manner. (I) mRNA-level analysis showing that hAMSC-Exos increased ANT2 expression in CTX-induced POI mice model with a dose-dependent manner. (J) mRNA-level analysis demonstrating that hAMSC-Exos improved AMPK expression in CTX-induced POI mice model with a dose-dependent manner. (K) mRNA-level analysis showing that hAMSC-Exos elevated L-OPA1 expression in CTX-induced POI mice model with a dose-dependent manner. (L) Protein-level analysis of hAMSC-Exos increased relative genes (ANT2, AMPK, and L-OPA1) expression in CTX-induced POI mice model with a dose-dependent manner. All experiments were repeated three times. Error bars indicate SD. ***$p < 0.001$.

chain reaction (qRT-PCR) assay showed that compared to the HDF control, hAMSC-Exos led to significantly increased miR-320a expression (Figure 3C). To confirm potential targets of miR-320a, we conducted bioinformatics predictions with a website (http://www.targetscan.org). According to the TargetScan analysis, the miR-320a target seed sequence in the 3′ untranslated region (3′ UTR) of SIRT4 is shown in Figure 3D, which is conserved among humans, mice, nonhuman primates, and cows (*Bos taurus*).

Exosomal miR-320a Recovered Ovarian Vitality, Increased Follicular Numbers, and Restored Hormonal Levels

To deeply explore the mechanism, we established knockdown of miR-320a in hAMSCs (hAMSC-Exos$^{anti\text{-}miR\text{-}320a}$), tested ovarian vitality (proliferation and apoptosis) by FACS, analyzed follicle regeneration by H&E staining, and detected the hormonal levels via the enzyme-linked immunosorbent assay (ELISA) method. We found that hAMSC-Exos stimulated ovarian proliferation and prohibited apoptosis. Stem cell therapy effects disappeared

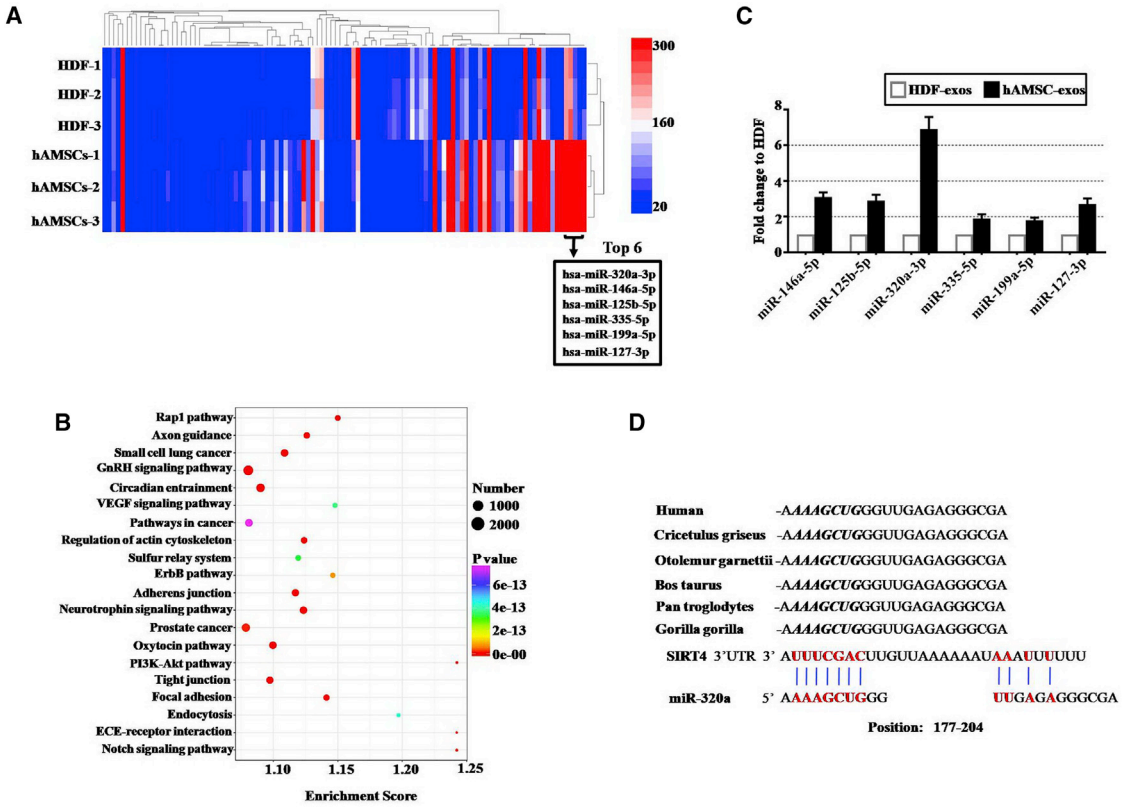

Figure 3. miRNA Profile of hAMSC-Exos

(A) The heatmap showing miRNA expression in three hAMSC-Exos samples and three HDF-Exos samples. The top 6 miRNAs enriched in hAMSC-Exos samples are highlighted in the square space. (B) KEGG analysis demonstrating the 20 top-ranked pathways enriched with miRNAs upregulated in hAMSC-Exos samples. (C) qRT-PCR method was used to detect miRNA expression in hAMSC-Exos and HDF-Exos samples. Our outcomes verified that miR-320a was highly expressed in hAMSC-Exos samples. Error bars indicate SD. (D) The sequence alignment of miR-320a and its predicted target sites of SIRT4 mRNA 3′ untranslated region (3′ UTR) are shown.

in the hAMSC-Exos$^{anti\text{-}miR\text{-}320a}$ group (Figures 4A and 4B). After hAMSC-Exos and hAMSC-Exos$^{anti\text{-}miR\text{-}320a}$ were separately injected into the ovaries, H&E staining revealed that the number of antral follicles and total follicular numbers were dramatically elevated to normal levels in the hAMSC-Exos group. Compared to the hAMSC-Exos groups, the hAMSC-Exos$^{anti\text{-}miR\text{-}320a}$-injected group did not show follicle regeneration as easily, as shown in Figures 4C and 4D. Quantification of hormonal levels revealed that hAMSC-Exos transplantation enhanced the E2 and AMH levels and decreased the FSH levels. There was hardly any change in the level of E2, AMH, and FSH after treatment with hAMSC-Exos$^{anti\text{-}miR\text{-}320a}$ in POI mice (Figures 4E–4G).

Exosomal miR-320a Inhibited SIRT4 Expression in Oocytes at Different Stages and Improved Follicular Marker Expression

In addition, immunofluorescence staining for SIRT4 in the process of oogenesis was also performed to detect the different stages (primordial, primary, secondary, and antral). As shown in Figure 5A, hAMSC-Exos repressed the expression of SIRT4 in POI ovaries at the four stages. The suppressive consequence for SIRT4 was not obvious in the hAMSC-Exos$^{anti\text{-}miR\text{-}320a}$ treatment group. Quantitative analysis of ovarian marker expression by FACS was carried out. The positive rates of FSHR^{+}/AMH^{+} (92.9%) and FOXL2^{+}/CYP19A1^{+} (84.5%) were higher in the hAMSC-Exos treatment group than in the POI group (12.0% and 19.3%), as shown in Figures 5B and 5C. hAMSC-Exos$^{anti\text{-}miR\text{-}320a}$ significantly diminished the change in the expression of markers that were observed in the hAMSC-Exos group.

Exosomal miR-320a Reduced the ROS Levels by Regulating SIRT4 in hGCs and Oocytes

To understand the relationship between exosomal miR-320a and ROS in POI disease, we employed FACS, ELISA, and immunofluorescence staining to determine the expression of ROS and SIRT4 in POI hGCs and oocytes. As shown in Figure 6A, the results from the FACS assay indicated that the ROS level was dramatically reduced in the POI hGCs after the hAMSC-Exos treatment compared to that in the POI group. In the hAMSC-Exos$^{anti\text{-}miR\text{-}320a}$ treatment group, the ROS level was the same as that in the POI group. High ROS levels accelerate energy metabolism impairment.[23] Therefore, we assessed the levels of energy storage and metabolism in POI hGCs in a starvation experiment. An ELISA revealed that the levels

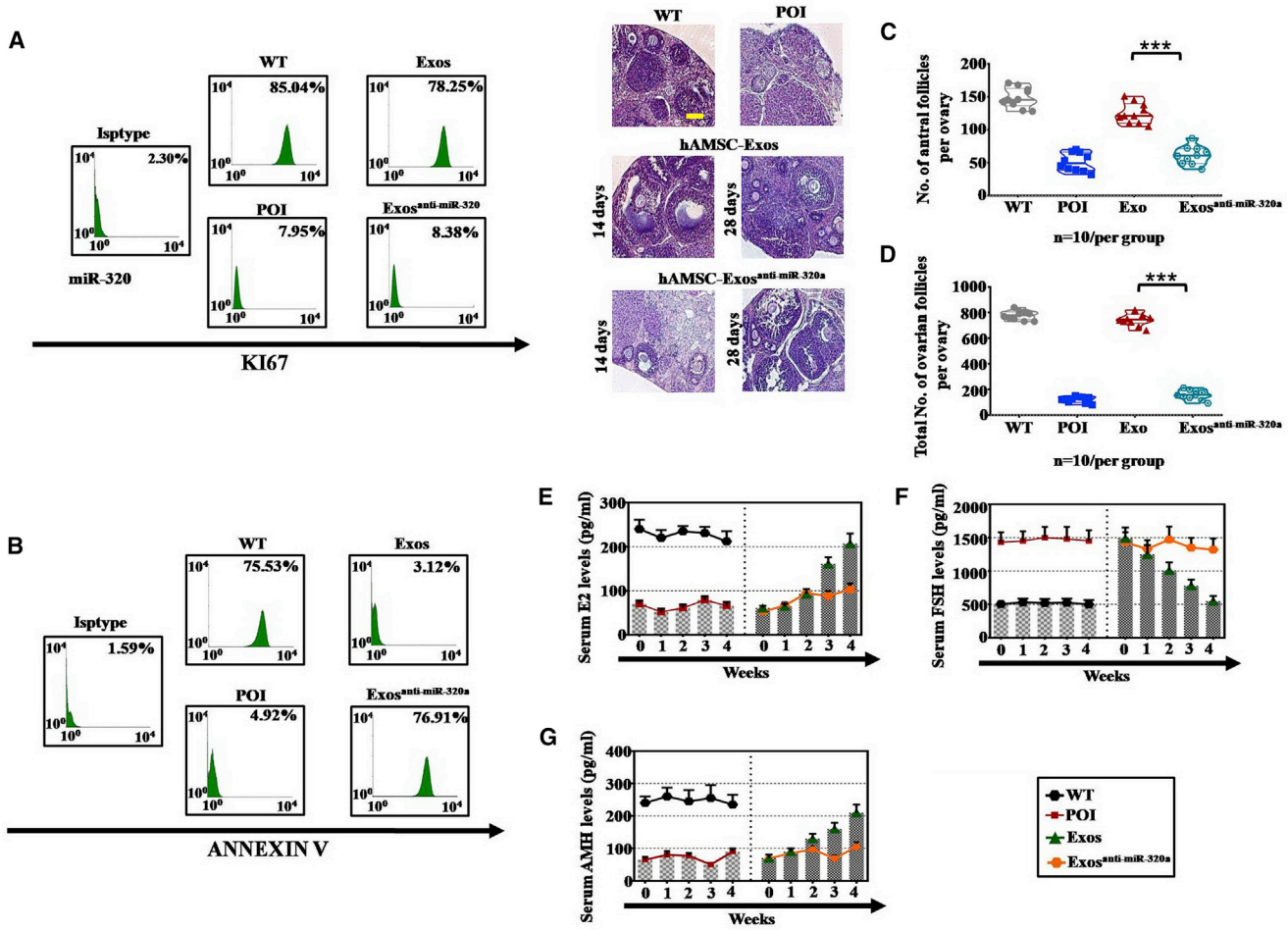

Figure 4. hAMSC-Exos Restored Follicular Number, Hormone Level, and Proliferation Rate in POI Mice Model by Releasing miR-320a

(A) FACS outcomes indicating that the KI67 expression was significantly elevated in in Exos/POI group than POI model group and Exos$^{anti\text{-}miR\text{-}320a}$/POI group. (B) FACS outcomes illustrating that the Annexin V expression was significantly downregulated in Exos/POI group than POI model group and Exos$^{anti\text{-}miR\text{-}320a}$/POI group. (C) H&E-staining showing the number of antral follicles in different groups at 14 and 28 days after transplantation. (D) H&E-staining showing the total number of ovarian follicles in different groups at 14 and 28 days after transplantation. ***$p < 0.001$. (E–G) Gonadal hormone parameters of mice in different groups after transplantation. Our results showed that the serum E2 levels were significantly elevated in Exos/POI group than POI model group and Exos$^{anti\text{-}miR\text{-}320a}$/POI group from 1 to 4 weeks posttransplantation (E). The serum FSH level was significantly repressed in Exos/POI group than POI model group and Exos$^{anti\text{-}miR\text{-}320a}$/POI group from 2 to 4 weeks post transplantation (F). The serum AMH levels were significantly elevated in Exos/POI group than POI model group and Exos$^{anti\text{-}miR\text{-}320a}$/POI group from 2 to 4 weeks posttransplantation (G). All experiments were repeated three times. Error bars indicate SD.

of TAG and glucose in the hAMSC-Exos treatment group were elevated compared to that in the POI hGCs after starvation for 72 h. This phenomenon was not observed in the hAMSC-Exos$^{anti\text{-}miR\text{-}320a}$ treatment group (Figures 6B and 6E). Discriminatively, the levels of glycogen and trehalose were reduced from 48 h to 72 h in the POI hGCs, and the treatment of hAMSC-Exos promoted the level of glycogen and trehalose; the therapeutic action of hAMSC-Exos was decreased when miR-320 was knocked down (Figures 6C and 6D). The expression levels of SIRT4 and ROS were also tested in POI oocytes. As shown in Figures 6F and 6G, immunofluorescence staining revealed that exosomes reduced the expression of SIRT4 and ROS dramatically, except for the hAMSC-Exos$^{anti\text{-}miR\text{-}320a}$ treatment group.

In addition, the phenotype of ovarian and embryo development was detected. When hAMSC-Exos were injected into the POI ovary, the weight was elevated compared to that of the hAMSC-Exos$^{anti\text{-}miR\text{-}320a}$ treatment group (Figure S2A). hAMSC-Exos and hAMSC-Exos$^{anti\text{-}miR\text{-}320a}$ did not change the formative rate of the 2-cell and morula stages in Figure S2B. The hAMSC-Exos group had a clearly increased litter size compared with that of the hAMSC-Exos$^{anti\text{-}miR\text{-}320a}$ treatment group (Figure S2C).

Exosomal miR-320a Maintains Ovarian Function and Inhibits ROS in POI Disease via SIRT4 Inhibition

To elucidate the mechanism behind these phenomena in ovarian function activated by hAMSC-Exos, we injected several

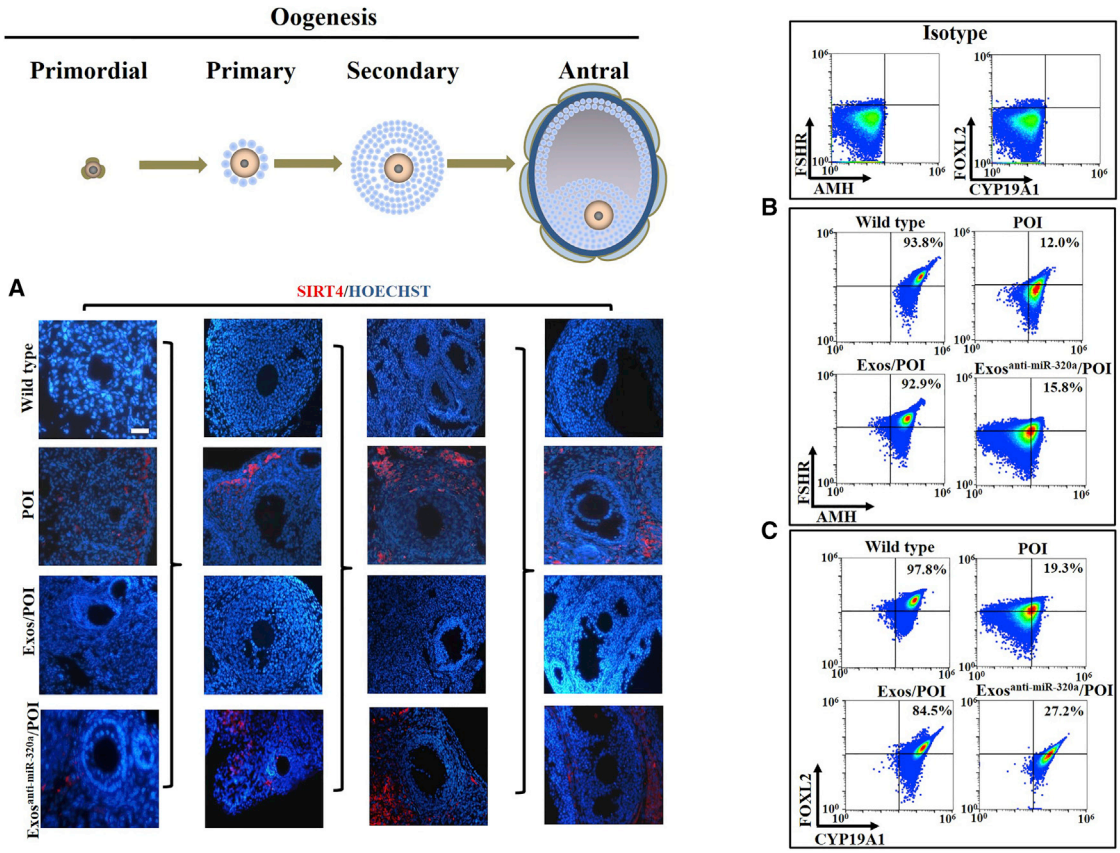

Figure 5. Exosomal miR-320a Improved Oogenesis and the Expression of Relative Genes

(A) Exosomes inhibited the expression of SIRT4 in POI group; the effectiveness was disappeared after miR-320a was knocked down. Scale bar, 20 μm. (B) FSHR^{+}/AMH^{+} cell number was increased in hAMSC-exosomal miR-320a treatment group. (C) hAMSC-exosomal miR-320a upregulated FOXL2^{+}/CYP19A1^{+} cell number in POI disease. hAMSC-Exos$^{anti\text{-}miR\text{-}320a}$ did not change the percentage. All experiments were repeated three times. Error bars indicate SD.

hAMSC-Exos$^{anti\text{-}miR\text{-}320a}$ and hAMSC-Exos into the ovaries. WB assays indicated that hAMSC-Exos decreased the protein expression of SIRT4, ANT2, AMPK, and L-OPA1 in the WT group in POI ovaries (Figures 7A–7D). The treatment effects were blocked when miR-320a was knocked down in the hAMSC-Exos group. The same results are also shown in the immunofluorescence assay. Exos inhibited SIRT4 and its downstream gene expression in the POI mouse model, except for in the hAMSC-Exos$^{anti\text{-}miR\text{-}320a}$ treatment group (Figures 7E and 7F). We also assessed the change in ROS levels in the hAMSC-Exos and hAMSC-Exos$^{anti\text{-}miR\text{-}320a}$ groups. Undoubtedly, hAMSC-Exos effectively inhibited the ROS levels in POI ovaries (15.91%) compared to that in the WT group (18.52%). The depressor effect was not found in the hAMSC-Exos$^{anti\text{-}miR\text{-}320a}$ treatment group, as shown in Figure 7G.

Exosomal miR-320a Induced Proliferation and Prohibited ROS by Regulating SIRT4 in hGCs

To further investigate the therapeutic mechanism of hAMSC-Exos miR-320a deeply, we cocultured hAMSC-Exos, hAMSC-Exos$^{anti\text{-}miR\text{-}320a}$, and the Exos inhibitor with hGCs. First, the suppressive effects of hAMSC-Exos in SIRT4 and its downstream genes were lowered after cotreatment with the hAMSC-Exos inhibitor. To detect whether hAMSC-Exos could deliver miR-320a to activate these signaling pathways, we cocultured hAMSC-Exos$^{anti\text{-}miR\text{-}320a}$ with POI hGCs. The same results as those due to treatment with the Exos inhibitor. hAMSC-Exos with low miR-320a expression exhibited an enhanced effect on the expression of SIRT4 and its downstream genes (Figures 8A–8D). We next sought to more precisely assay the relationship between exosomal miR-320 and SIRT4 with hGC-SIRT4^{KD} and hGC-SIRT4^{OE} cell lines. Gratifyingly, the upregulated expression of SIRT4 and its downstream genes from hAMSC-Exos were individually reduced by the Exos inhibitor in hGCs-SIRT4^{KD} (Figures 8E–8H) and hGCs-SIRT4^{OE} (Figures 8I–8L). hAMSC-Exos$^{anti\text{-}miR\text{-}320a}$ also lost the elevated ability of SIRT4 and its downstream genes, as shown in Figures 8E–8L. In addition, more effective hAMSC-Exos inhibited ROS levels in hGCs-SIRT4^{KD} (Figure 8M) and hGCs-SIRT4^{OE} (Figure 8N). The hAMSC-Exos repressive role for ROS was impeded after miR-320a knockdown (Figures 8M and 8N). These data suggest that hAMSC-Exos can enhance POI ovarian function by targeting SIRT4 through miR-320a.

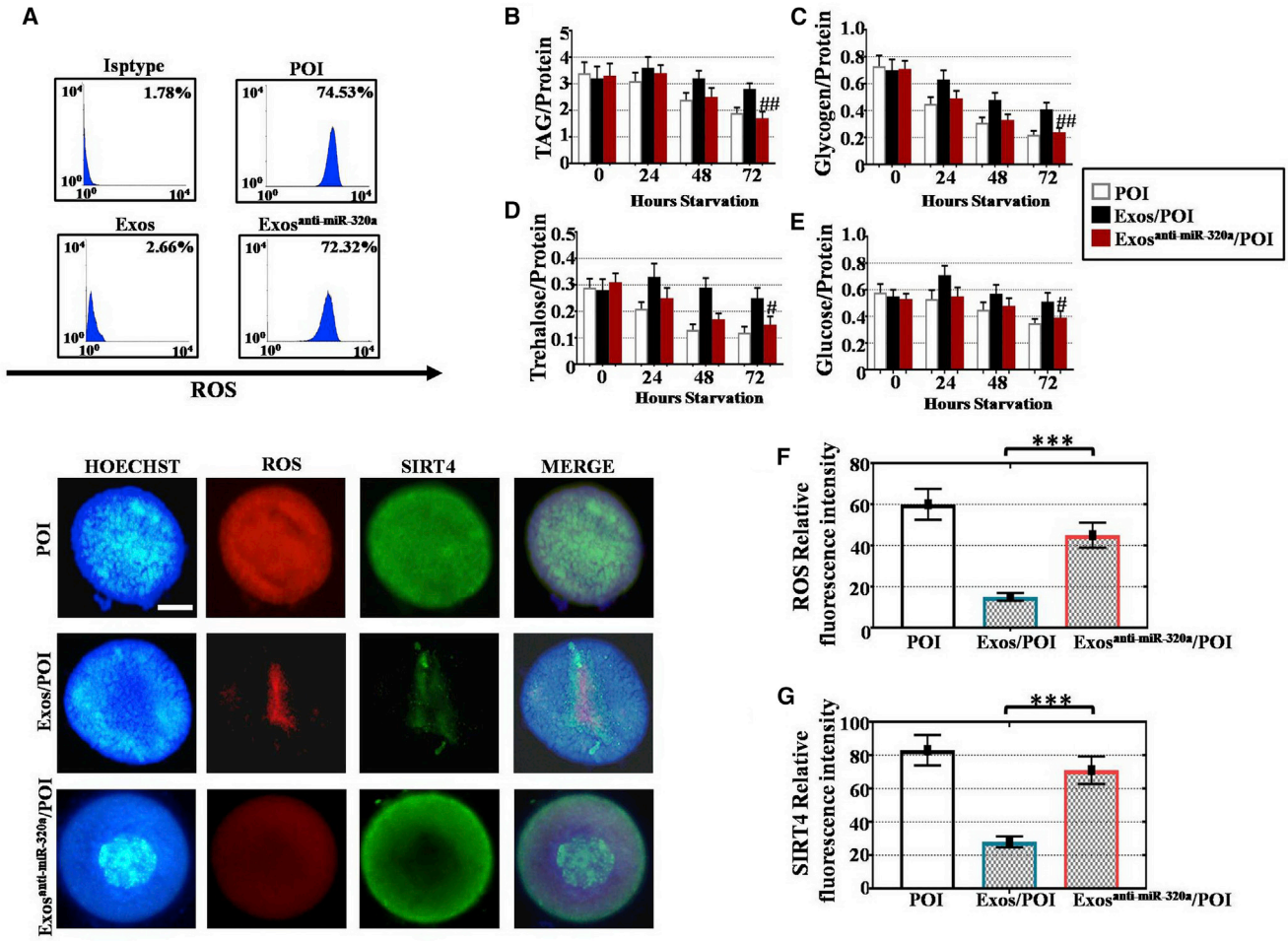

Figure 6. Exosomal miR-320a Repressed ROS in POI hGCs and Oocytes

(A) FACS outcomes showing that ROS was dramatically repressed in CTX-damaged hGCs treated with hAMSC-Exos (Exos/POI) than CTX-damaged hGCs treated with PBS (POI) and CTX-damaged hGCs treated with hAMSC-Exos$^{anti\text{-}miR\text{-}320a}$ (Exos$^{anti\text{-}miR\text{-}320a}$/POI). (B) Spectrophotometer analysis indicating the significantly elevated expressions of TAG in CTX-damaged hGCs treated with hAMSC-Exos (Exos/POI) than POI group and hAMSC-Exos $^{anti\text{-}miR\text{-}320a}$ group (Exos$^{anti\text{-}miR\text{-}320a}$/POI) from 24 to 48 h post-treatment. (C) Spectrophotometer analysis indicating the significantly elevated expressions of glycogen in CTX-damaged hGCs treated with hAMSC-Exos (Exos/POI) with a time-dependent manner. (D) Spectrophotometer analysis indicating the significantly elevated expressions of trehalose in CTX-damaged hGCs treated with hAMSC-Exos (Exos/POI) with a time-dependent manner. (E) Spectrophotometer analysis indicating the significantly elevated expressions of glucose in CTX-damaged hGCs treated with hAMSC-Exos (Exos/POI) with a time-dependent manner. (F) Immunocytochemical images and quantitative analysis of fluorescence intensity showing significantly down-regulated ROS expression in hAMSC-Exos-treated POI oocytes than POI oocytes and hAMSC-Exos$^{anti\text{-}miR\text{-}320a}$-treated POI oocytes. (G) Immunocytochemical images and quantitative analysis of fluorescence intensity showing significantly downregulated SIRT4 expression in hAMSC-Exos-treated POI oocytes than POI oocytes and hAMSC-Exos$^{anti\text{-}miR\text{-}320a}$-treated POI oocytes. Scale bar, 10 μm. ***$p < 0.001$. All experiments were repeated three times. Error bars indicate SD. #$p < 0.05$, ##$p < 0.01$.

DISCUSSION

At present, many reports have indicated the therapeutic action of perinatal stem cells (PSCs) for POI disease.[24,25] Little research has been conducted on the relationship between aging and PSC-exosomal miRNAs. hGCs are essential components of ovarian follicles, playing a supportive and nutritive role in the oogenesis and the development of oocytes. The present study was the first to report that hAMSC-Exos exhibit a reverse apoptotic effect in chemotherapy-induced premature ovarian failure (POF) hGCs and ovaries (Figures 1 and 2). A previous study demonstrated that MSC-Exos improved anti-apoptosis and tissue regeneration potency in myocardial infarction disease.[26]

To determine the regulation of the mechanism, we measured the expression of SIRT4 and relative genes (ANT2, AMPK, and L-OPA1) and found that they were highly expressed in POI hGCs and ovaries. In our study, hAMSC-Exos decreased the expression of SIRT4, AMPK, ANT2, and L-OPA1 *in vivo* and *in vitro* experiments (Figures 1 and 2). Our results are consistent with early studies and show that SIRT4 overexpression accelerated the aging process in

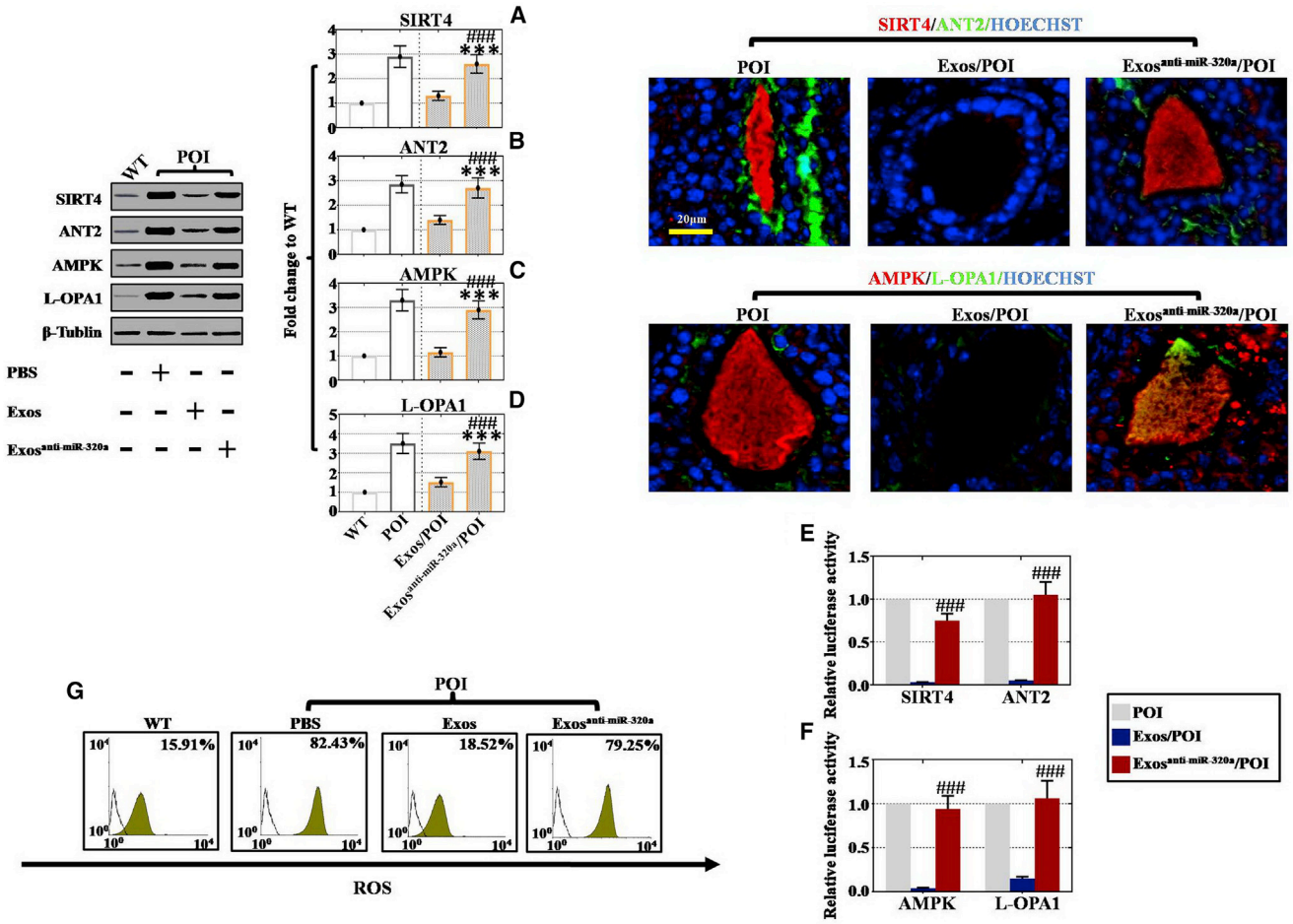

Figure 7. Exosomal miR-320a Repressed ROS through Regulating SIRT4 in POI Mice Model

(A) WB results indicating that SIRT4 expression was significantly downregulated in mouse ovarian of Exos/POI group than POI model group and Exos$^{anti\text{-}miR\text{-}320a}$/POI group. (B) Protein-level analysis of ANT2 showing that was downregulated in Exos/POI group than POI model group and Exos$^{anti\text{-}miR\text{-}320a}$/POI group. (C) Protein-level analysis of AMPK showing that was inhibted in Exos/POI group than POI model group and Exos$^{anti\text{-}miR\text{-}320a}$/POI group. (D) Protein-level analysis of L-OPA1 showing that was decreased in Exos/POI group than POI model group and Exos$^{anti\text{-}miR\text{-}320a}$/POI group. (E) Fluorescence microscopy images and quantitative analysis of fluorescence intensity showed decreased expressions of SIRT4 (red) and ANT2 (green) in mouse ovarian of Exos/POI group than POI model group and Exos$^{anti\text{-}miR\text{-}320a}$/POI group. Scale bar, 20 μm. (F) Fluorescence microscopy images and quantitative analysis of fluorescence intensity showed decreased expressions of AMPK (red) and L-OPA1 (green) in mouse ovarian of Exos/POI group than POI model group and Exos$^{anti\text{-}miR\text{-}320a}$/POI group. Scale bar, 20 μm. (G) FACS outcomes showed dramatically repressed ROS in mouse ovarian of Exos/POI group than POI model group and Exos$^{anti\text{-}miR\text{-}320a}$/POI group. All experiments were repeated three times. Error bars indicate SD. ***$p < 0.001$, ###$p < 0.001$.

oocytes.[20] Elevated SIRT4-OPA1 axis is linked to the phenomenon of aging-associated mitochondrial dysfunction.[27]

Interest in MSC-Exos has greatly expanded with recent discoveries that miRNAs are present and are transferred to target cells to regulate cell-to-cell communication and the recipient cell's functions.[27] Many studies have indicated that exosomes also play important roles in the regulation of biological function in various aspects of dysgenesis, including embryo development, gametogenesis, and fertilization.[28,29] Therefore, our results focus on the effects of exosomal miRNAs. For further analysis of the composition of hAMSC-Exos, miRNA microarray assays were carried out. Although the miRNAs were predicted to target genes mainly enriched in the PI3K-AKT. Previous studies demonstrated that AMPK exerted regulatory effects on the PI3K pathway.[30,31] Phosphatase and tensin homolog (PTEN) plays a critical role in cell proliferation by regulating the PI3K-AKT pathway.[32] According to a previous study, lack of SIRT4 activated AMPK expression,[21] and SIRT4 could regulate cell survival by affecting stability of PTEN.[33] Therefore, the possible reason for regulatory genes mainly enriched in the PI3K may due to indirect regulation by SIRT4. Besides, the high expression of miR-320a in hAMSC-Exos is shown in Figure 3, and we also found that the miR-320a was highly target seed sequence in the 3′ UTR of SIRT4. The results of the experiment also indicated that hAMSC-Exos promote follicular numbers, hormone levels, and oogenesis by releasing miR-320a (Figures 4 and 5). SIRT4 has been identified as a direct target of miR-320a through

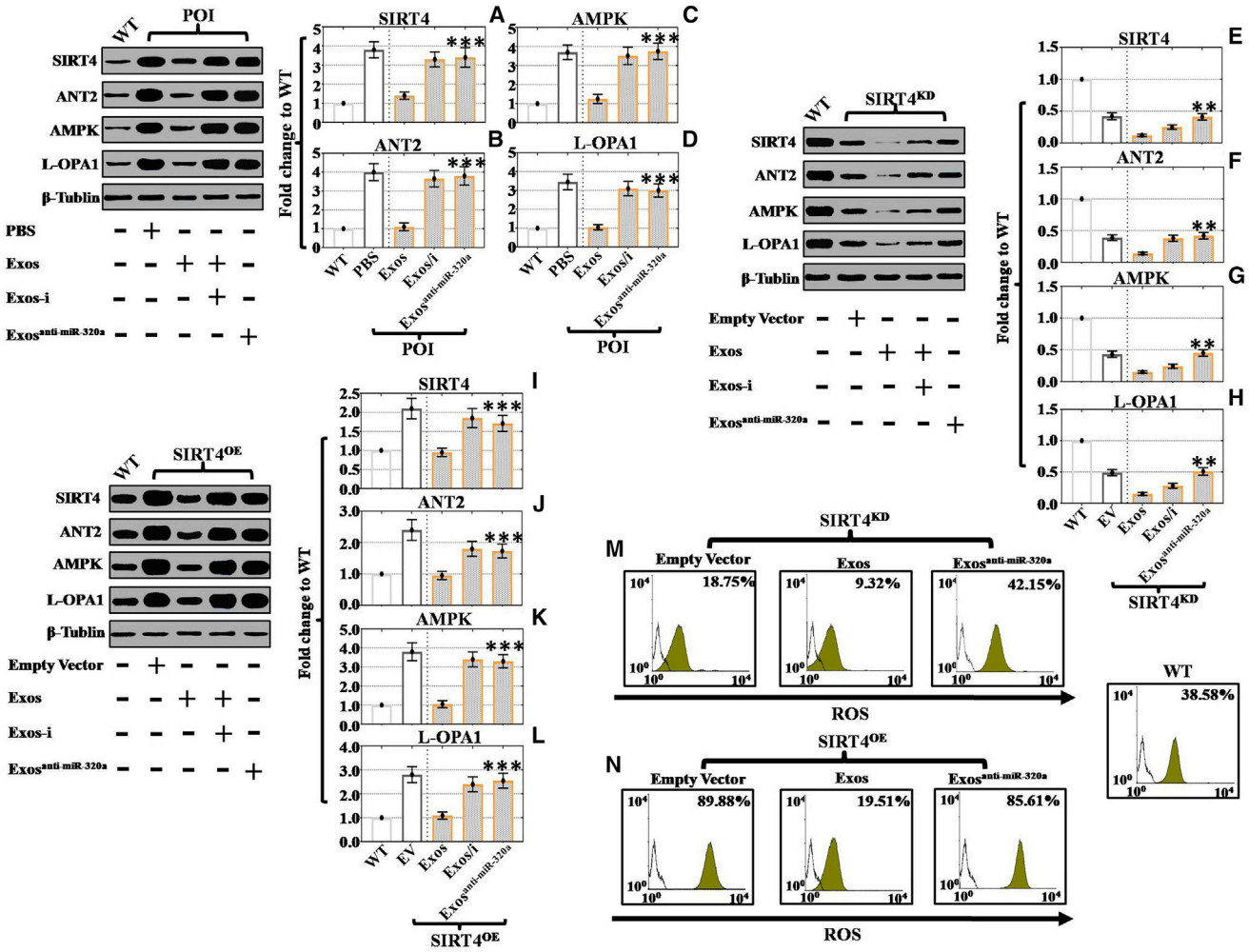

Figure 8. Exosomal miR-320a Repressed ROS in hGCs-SIRT4^{KD} and hGCs-SIRT4^{OE} through Regulating SIRT4

(A) WB results indicated that SIRT4 expression was significantly downregulated in CTX-damaged hGCs treated with hAMSC-Exos than PBS, Exos-inhibitor, and hAMSC-Exos$^{anti\text{-}miR\text{-}320a}$. (B) Protein-level analysis of ANT2 showed that expression was downregulated in CTX-damaged hGCs treated with hAMSC-Exos than Exos-inhibitor and hAMSC-Exos$^{anti\text{-}miR\text{-}320a}$. (C) Protein-level analysis of AMPK showed that expression was decreased in CTX-damaged hGCs treated with hAMSC-Exos than Exos-inhibitor and hAMSC-Exos$^{anti\text{-}miR\text{-}320a}$. (D) Protein-level analysis of L-OPA1 showed that expression was inhibited in CTX-damaged hGCs treated with hAMSC-Exos than Exos-inhibitor and hAMSC-Exos$^{anti\text{-}miR\text{-}320a}$. (E) WB results showed reduced SIRT4 expression in hGCs-SIRT4^{KD} treated with hAMSC-Exos, except for Exos-inhibitor and hAMSC-Exos$^{anti\text{-}miR\text{-}320a}$. (F) hAMSC-Exos decreased protein-level of ANT2 in hGCs-SIRT4^{KD}, except for Exos-inhibitor and hAMSC-Exos$^{anti\text{-}miR\text{-}320a}$ treatment group. (G) hAMSC-Exos inhibited protein-level of AMPK in hGCs-SIRT4^{KD}, except for Exos-inhibitor and hAMSC-Exos$^{anti\text{-}miR\text{-}320a}$ treatment group. (H) hAMSC-Exos prohibited protein-level of L-OPA1 in hGCs-SIRT4^{KD}, except for Exos-inhibitor and hAMSC-Exos$^{anti\text{-}miR\text{-}320a}$ treatment group. (I) hGC-SIRT4^{OE} treated with extracellular vesicles (EV), Exos-inhibitor, and hAMSC-Exos$^{anti\text{-}miR\text{-}320a}$. WB results showed that lower expression of SIRT4 can be observed in hGCs-SIRT4^{OE} treated with hAMSC-Exos than EV, Exos-inhibitor, and hAMSC-Exos$^{anti\text{-}miR\text{-}320a}$. (J) The expression of ANT2 was dramatically downregulated in CTX-damaged hGC-SIRT7^{OE} treated with hAMSC-Exos than EV, Exos-inhibitor, and hAMSC-Exos$^{anti\text{-}miR\text{-}320a}$ group. (K) The expression of AMPK was dramatically inhibited in CTX-damaged hGC-SIRT7^{OE} treated with hAMSC-Exos than EV, Exos-inhibitor, and hAMSC-Exos$^{anti\text{-}miR\text{-}320a}$ group. (L) The expression of L-OPA1 was dramatically suppressed in CTX-damaged hGC-SIRT7^{OE} treated with hAMSC-Exos than EV, Exos-inhibitor, and hAMSC-Exos$^{anti\text{-}miR\text{-}320a}$ group. (M) FACS assay revealing that reduced SIRT4 expression elevated oxidative stress level. The ROS level was dramatically downregulated in hGCs-SIRT4^{KD} treated with hAMSC-Exos than hAMSC-Exos$^{anti\text{-}miR\text{-}320a}$. (N) The ROS level was dramatically downregulated in hGCs-SIRT7^{OE} treated with hAMSC-Exos than hAMSC-Exos$^{anti\text{-}miR\text{-}320a}$. All experiments were repeated three times. Error bars indicate SD. **$p < 0.01$, ***$p < 0.001$.

bioinformatics prediction. We knocked down miR-320a in hAMSCs to determine the interaction between exosomal miR-320a and SIRT4 in aging resistance in POI oocytes, hGCs, and ovaries. In an *in vivo* and *in vitro* study, hAMSC-Exos without miR-320a delivery did not alter the expression of SIRT4 or the ROS levels (Figures 6,7, and 8). A previous study supported our results that miR-320a may play a key role in preventing the upregulation of glycolysis and the associated ROS-induced pathological disease,[34,35] which is involved in MII oocyte development and embryo quality,[36] and embryo quality is related to the influence of proliferation in mouse hGCs.[37] In

contrast, hAMSC-Exos inhibited the protein expression of SIRT4, ANT2, AMPK, and L-OPA1. Then, the level of ROS was also reduced. Knockdown of miR-320a in hAMSCs revealed that the regulatory ability of exosomal miR-320a failed. Furthermore, we also found suppression of genes (ANT2, AMPK, and L-OPA1) in hGCs-SIRT^{KD} and promotion in hGCs-SIRT^{OE}. These results suggest that ANT2, AMPK, and L-OPA1 are downstream genes for SIRT4 (Figures 7 and 8).

In summary, this study integrates systems biology analysis and bioexperiments to predict and confirm that exosomal miR-320a is responsible for hAMSC resistance to ovarian senilism. In addition, we revealed that exosomal miR-320a may retard POI and reduce the ROS levels by regulating SIRT4 by delivering exosomal miR-320a to the POI oocyte, hGCs, and ovaries (Figure S3). This study suggests that modulation of miR-320a expression in MSCs may serve as a therapeutic approach to POI disease.

MATERIALS AND METHODS

Isolation and Culture of hAMSCs

According to our previous study, the cell line from hAMSCs was stably obtained.[6] Brief details are described below: digested cells were planted in a 10 cm^2 culture dish with a concentration of $1 \times 10^7/cm^2$ and cultured in an incubator at 37°C with 5% CO_2. Isolated cells were fed every third day. After removing the nonadherent cells, hAMSCs were obtained. Cells from passages 3–5 were used for this study.

Isolation of Primary hGCs from POI Patients

hGCs were voluntarily donated from POI patients. The ethics committee of Suzhou Municipal Hospital approved the use of hGCs for the following experiments. All patients were informed, and written consent was signed. All information about samples and patients was anonymized. After centrifugation at 560 × *g* for 3 min, hGCs were isolated. Then, hGCs were washed in serum-free DMEM/F12 media 3 times. Next, hGCs were cultured in DMEM/F12 media supplemented with 10% fetal bovine serum (FBS). The following experiments were conducted on the third day after cell culture.

Preparation of hAMSC-Exos

Secretory exosomes from the culture medium of hAMSCs were obtained. In detail, hAMSCs at passage 3 were seeded onto culture plates and reached 80% confluence at 5 days. Then, the conditioned medium with exosome-depleted FBS (Thermo Fisher, USA) was collected after culturing for 48 h. To remove cells, we centrifuged the collected medium at 300 × *g* for 10 min at 4°C followed by filtration through 0.22 μm filters. Then, the supernatant was centrifuged at 3,000 × *g* for 15 min at 4°C to filter cells and debris again. The supernatant was collected carefully and mixed with ExoQuick precipitation solution (SBI, USA). After incubating overnight at 4 °C, exosomes were isolated by centrifuging at 1,500 × *g* for 30 min at 4 °C. The formed exosome pellet was dissolved in PBS before being added to the culture medium of CTX-damaged hGCs. The exosomes were labeled with CM-Dil Dye (Sigma-Aldrich, USA), a molecular probe, following the manufacturer's instructions, before being injected into the POI mouse model.

Electron Microscopy Analysis of hAMSC-Derived Exosomes

The hAMSC-derived exosomes were resuspended in 30 μL PBS. Each 10 μL hAMSC-Exos sample was loaded on copper grids. Then, 1% (w/v) phosphotungstic acid (PTA, Electron Microscopy Sciences, USA) was used to stain hAMSC-Exos for 1 min at room temperature. Images of exosomes were taken by transmission electron microscopy (HITACH, Japan).

miRNA Library Construction and Sequencing

miRNAs of exosomes derived from hAMSCs and HDF (human dermal fibroblast) were extracted using the exoEasy Maxi Kit (-QIAGEN, Germany). The quantity of RNA yield was measured by Qubit 2.0 (Life Technologies, USA), and the integrity was confirmed by Agilent 2100 TapeStation (Agilent Technologies, USA). A total of 50 ng of total exosomal RNA from each sample was used for small RNA library preparation. NEBNext, Multiplex Small RNA Library Prep Set for Illumina (New England Biolabs, USA) was used, and small RNA sequencing was conducted by HiSeq 2500 (Illumina, USA) with reads lengths from 15 to 55 bp. The miRNA expression level was calculated and normalized by RPM values as per million mapped reads. CLC Genomics Workbench was used to further analyze miRNA-seq outcomes.

Reverse Transcription and qRT-PCR

The expression levels of miR-146-5p, miR-125b-5p, miR-320a-3p, miR-335-5p, miR-199a-5p, and miR-127-3p in hAMSC-Exos and HDF-Exos, ANT2, AMPK, and L-OPA1 in POI hGCs and ovaries were verified by qRT-PCR. Total RNA was extracted using TRIzol. Then, the RNA template was reverse transcribed into cDNA using the miScript II RT Kit (QIAGEN, Netherlands). qRT-PCR was performed using the miScript SYBR Green PCR Kit (QIAGEN, Netherlands) following the manufacturer's instructions. The mRNA and miRNA expression levels were analyzed by a CFX96 Touch Real-Time PCR Detection System (Bio-Rad, CA). The primer sequences used are listed in Table S4.

Experimental Animals and POI Mouse Model Establishment

All the experimental procedures in this study were conducted following the recommendations of the association for research in reproductive function and was approved by the Ethics Committee of Nanjing Medical University (approval number: 20170480). 10-week-old female specific pathogen-free (SPF) grade C57B6L/J mice were purchased from the Institute of Animal Research in Nanjing Medical University. According to our previous study,[6] after cyclophosphamide (120 mg/kg) treated the mice 2 weeks, POI mouse model was established. In this study, mice were equally and randomly divided into four groups: wild-type mice (WT group, n = 10), CTX-induced POI model mice (POI group, n = 10), CTX-induced POI model mice treated with exosomes from hAMSCs (Exos/POI group, 100 μL of PBS containing the 150 μg exosomes, n = 10), and CTX-induced POI model mice treated with exosomes from

hAMSC-miR-320a^{KD} (Exos$^{anti\text{-}miR\text{-}320a}$/POI group, n = 10). The WT mice were not given any treatment. To establish the POI mouse model, we performed an intraperitoneal injection of 120 mg/kg CTX (Sigma, USA).[6] At least three biological repetitions were conducted during the experiments. Operators were blinded to the treatment during data analysis and acquisition. The survival rate was monitored every month for 1 year.

FACS Analysis

Approximately 2 × 10^6 hGCs or ovarian cells were washed with warmed Dulbecco's phosphate-buffered saline (DPBS) followed by digestion in 0.25% trypsin. Then, 2 × 10^5 cells were stained with PE-conjugated or fluorescein isothiocyanate (FITC)-conjugated antibodies (Table S1). Recommended isotype controls were used to set negative controls. Each sample was washed with DPBS 3 times before being resuspended in 100 μL loading buffer. The marker expression in each sample was then detected by a fluorescence-activated cell sorter (Beckman, USA) and analyzed by FlowJo. When intracellular proteins were detected, cells were fixed for 30 min at room temperature. Then, cells were permeated with Cytofix/Cytoperm Fixation/Permeabilization Solution Kit (BD, USA). At least three assays were performed for each experiment.

WB Analysis

hGCs or ovarian cells were lysed with lysis buffer (Beyotime Biotechnology, China). Then, 20 μg of protein was extracted and loaded onto 10% gels and fractioned via 10% or 20% SDS-PAGE (sodium dodecyl sulfate-polyacrylamide gel electrophoresis). Next, the separated proteins were electroblotted onto polyvinylidene difluoride (PVDF) membranes (Millipore, USA). The membranes were incubated with primary antibodies at 4°C overnight (Table S2) followed by incubation with secondary antibodies for 2 h at room temperature. The protein-level marker expression of each sample was detected with enhanced chemiluminescence (Pierce ECL western blotting substrate, Thermo Fisher, USA) and scanned by a chemiluminescence detection system (Tanon, China). ImageJ software (National Institutes of Health, USA) was used to analyze the signal intensity of the band of interest in the grayscale images. Experiments were repeated three times. The results are presented as the fold change ± SD.

Immunofluorescence Staining

Oocytes from the CTX-induced POI mouse model were fixed on cell glass slides for immunofluorescence staining. The cells were washed with PBS 3 times before fixation in 4% paraformaldehyde at room temperature for 30 min. Cells were permeated with PBST (PBS with 0.3% Triton X-100) at room temperature for 30 min. Then, cell slides were washed with PBS 3 times and blocked with 5% BSA for 1 h at room temperature. After another wash 3 times, the primary antibodies (Table S3) were incubated with oocytes or ovarian tissues overnight at 4°C. After being washed with PBS 3 times, the cells were incubated with a secondary antibody for 40 min at room temperature. Finally, Hoechst-Fluoromount-G (Southern Biotech, USA) was added to the cell slides to preserve the immunofluorescent labels before mounting. Selected paraffin-embedded mouse ovarian sections were subjected to dewaxing and antigen retrieval. Then, the paraffin sections were treated with PBST (PBS with 0.3% Triton X-100) at room temperature for 60 min and blocked in 5% BSA for 1 h at room temperature. This process was followed by overnight incubation with a diluted primary antibody at 4°C. The binding of the primary antibodies was tested by washing and incubating the slides with a secondary antibody for 40 min at room temperature. Mice sections were mounted using Hoechst-Fluoromount-G (Southern Biotech, USA) and viewed under a Nikon Eclipse E800 microscope. Images were captured using an Olympus digital camera (Shinjuku district, Tokyo, Japan). Information concerning the primary antibodies used is provided in Table S3. Three or four samples were analyzed for each group.

Gene Silencing via RNA Interference

For SIRT4 knockdown, hGCs were transfected with small interfering RNA (siRNA; Thermo Fisher, USA) targeting human SIRT4 using Lipofectamine 2000 (Invitrogen, USA) following the manufacturer's instructions. A nonsilencing scrambled siRNA was used to set up the negative control. WB analysis was performed to verify the knockdown efficiency by detecting target protein levels.

Gene Overexpression via Retrovirus Transduction

To overexpress SIRT4 in hGCs, we amplified the SIRT4 coding sequence from human gDNA. Then, we cloned the SIRT4 coding sequence into the BglII and SalI sites of the retroviral vector from the pLNCX2 virus (Clontech, USA) with a multiplicity of infection (MOI) of 5. Retrovirus transduction was performed by culturing hGCs with retrovirus or control plasmids in a 37°C incubator with 5% CO_2 for 48 h. Then, the cells were centrifuged at 1,000 × *g* for 10 min to remove residual retrovirus in the supernatant. Next, hGCs were cultured with medium containing 1,000 mg/mL G418 for 2 weeks to select retrovirus-infected cells. SIRT4 overexpression was measured by detecting the target protein levels.

miRNA Knockdown

To knock down miR-320a expression, we transfected anti-miR-320a oligonucleotides (RiboBio, China) into hAMSCs using ribo FECT CP Transfection Kits (RiboBio, China). Anti-miR-320a oligonucleotides were added to hGC culture medium for 24 h. Then, fresh medium was added, and hGC$^{anti\text{-}miR\text{-}320a}$ was further cultured to 80% confluence. To collect Exos$^{anti\text{-}miR\text{-}320a}$, we cultured hAMSCs$^{anti\text{-}miR\text{-}320a}$ in medium with exosome-depleted FBS for 48 h. Next, the supernatant was extracted and the exosomes were isolated.

Ovarian Follicle Count

At 4 weeks posttransplantation, the mice were euthanized, and both ovaries from each mouse were isolated and fixed in 10% paraformaldehyde for 2 h. Then, the ovaries were embedded in paraffin and sectioned to a thickness of 5 μm. Five sections were collected from each ovary. The ovarian structure and follicle phenotype were shown by staining with H&E. Total follicles and antral follicles were classified. Every follicle containing an oocyte was counted once to avoid recounting. Every experiment was repeated at least three times. The results are presented as the fold change ± SD.

Metabolite Assay

For the metabolite assay, 0, 24, 48, and 72 h cultured hGCs were extracted. Protein levels of triglyceride (Triglyceride Assay Kit, Abcam, USA), glycogen (Glycogen Assay Kit II, Abcam, USA), trehalose (Trehalose, Assay Kit, MYBioSource, USA), and glucose (Glucose Assay Kit, Abcam, USA) were qualified by a spectrophotometer (Varian Company, Australia) following the manufacturer's instructions. A minimum of three assays were performed, and the outcomes are shown as the fold change ± SD.

ELISA Analysis

For the hormone assay, the levels of serum E2, FSH, and AMH in the mouse model and 0.5 mL blood samples were obtained by retroorbital puncture under anesthesia. Blood samples were centrifuged at 4,000 r/min for 10 min to remove the cells. Then, the supernatant was isolated and incubated. The concentrations of the hormones were detected by ELISA kits following the manufacturer's instructions. Briefly, 50 μL serum sample was added into each well and incubated for 30 min at 37°C. Then, Wash Buffer was used to wash wells 5 times before incubating with HRP-conjugated reagent for 60 min at 37°C. After another 5 washes with Wash Buffer, Substrate A and B Solutions were added to each well and incubated for 15 min at 37°C. Finally, immediately after Stop Solution was added to each well, samples were measured by a spectrophotometer (Varian Company, Australia). Each sample was detected using three wells, and the results are shown as the fold change ± SD.

hGC Starvation Assays

hGCs were seeded on culture plates and cultured in DMEM with 10% FBS for 12–16 h to allow cell attachment. Next, media and nonadherent cells were removed. To starve hGCs, we cultured cells with fresh medium without FBS for 24 h.

Statistical Analysis

All experiments in this study were repeated a minimum of 3 times. The values are shown as the mean ± SD. Before Scheffe's t test (SPSS 21.0 software) was conducted, one-way ANOVA was performed. Probability values <5% were considered significant.

SUPPLEMENTAL INFORMATION

Supplemental Information can be found online at https://doi.org/10.1016/j.omtn.2020.05.013.

AUTHOR CONTRIBUTIONS

C.D. and C.Q. performed the cellular and molecular assays *in vivo* and *in vitro*. Q.Z. participated in the statistical analysis and revised the manuscript. S.H. contributed to hGC and exosomes collection and purification. Q.Z. contributed to hGC purification culture. C.D. carried out the partial immunoassays. J.L. carried out the partial H&E assays. C.Q. participated in the mice feeding. B.H. planned the experiments and drafted part of the manuscript. B.H. and H.L. planned the experiments and wrote the manuscript. All the authors read and approved the final manuscript.

CONFLICTS OF INTEREST

The authors declare no competing interests.

ACKNOWLEDGMENTS

This work was supported by the grants from National Natural Science Foundation of China (81801515 and 81801494), Suzhou Introduce Expert Team of Clinical Medicine (SZYJTD201708, SZYJTD201707), Suzhou Talent Training Program (GSWS2019005), and Suzhou Science and Technology for People's Livelihood (SYS2018081). The authors would like to thank Dr. Qidong Zu (OE Biotech, Shanghai, China) for assistance with the bioinformatics analysis of the sequencing data. The use of human ovarian granular cells was in accordance with the relevant guidelines and regulations and the experimental protocols were approved by the Medical Ethics Committee of the Suzhou Hospital Affiliated to Nanjing Medical University (SZ-NJMU-003). All the patients provided written informed consent prior to participation in this study. Our investigation using experimental animals was conducted on the basis of the Nanjing Medical University Animal Center's specific guidelines and standards (20170480).

REFERENCES

1. Qin, Y., Jiao, X., Simpson, J.L., and Chen, Z.J. (2015). Genetics of primary ovarian insufficiency: new developments and opportunities. Hum. Reprod. Update *21*, 787–808.

2. Jiao, X., Ke, H., Qin, Y., and Chen, Z.J. (2018). Molecular Genetics of Premature Ovarian Insufficiency. Trends Endocrinol. Metab. *29*, 795–807.

3. Wang, Y., Chen, X., Cao, W., and Shi, Y. (2014). Plasticity of mesenchymal stem cells in immunomodulation: pathological and therapeutic implications. Nat. Immunol. *15*, 1009–1016.

4. Ding, C., Zou, Q., Wang, F., Wu, H., Wang, W., Li, H., and Huang, B. (2018). HGF and BFGF Secretion by Human Adipose-Derived Stem Cells Improves Ovarian Function During Natural Aging via Activation of the SIRT1/FOXO1 Signaling Pathway. Cell. Physiol. Biochem. *45*, 1316–1332.

5. Ding, L., Li, X., Sun, H., Su, J., Lin, N., Péault, B., Song, T., Yang, J., Dai, J., and Hu, Y. (2014). Transplantation of bone marrow mesenchymal stem cells on collagen scaffolds for the functional regeneration of injured rat uterus. Biomaterials *35*, 4888–4900.

6. Ding, C., Li, H., Wang, Y., Wang, F., Wu, H., Chen, R., Lv, J., Wang, W., and Huang, B. (2017). Different therapeutic effects of cells derived from human amniotic membrane on premature ovarian aging depend on distinct cellular biological characteristics. Stem Cell Res. Ther. *8*, 173.

7. Phinney, D.G., and Pittenger, M.F. (2017). Concise Review: MSC-Derived Exosomes for Cell-Free Therapy. Stem Cells *35*, 851–858.

8. Zhang, Y., Kim, M.S., Jia, B., Yan, J., Zuniga-Hertz, J.P., Han, C., and Cai, D. (2017). Hypothalamic stem cells control ageing speed partly through exosomal miRNAs. Nature *548*, 52–57.

9. Huang, B., Lu, J., Ding, C., Zou, Q., Wang, W., and Li, H. (2018). Exosomes derived from human adipose mesenchymal stem cells improve ovary function of premature ovarian insufficiency by targeting SMAD. Stem Cell Res. Ther. *9*, 216.

10. Sun, L., Li, D., Song, K., Wei, J., Yao, S., Li, Z., Su, X., Ju, X., Chao, L., Deng, X., et al. (2017). Exosomes derived from human umbilical cord mesenchymal stem cells protect against cisplatin-induced ovarian granulosa cell stress and apoptosis in vitro. Sci. Rep. *7*, 2552.

11. Hu, Y., Rao, S.S., Wang, Z.X., Cao, J., Tan, Y.J., Luo, J., Li, H.M., Zhang, W.S., Chen, C.Y., and Xie, H. (2018). Exosomes from human umbilical cord blood accelerate cutaneous wound healing through miR-21-3p-mediated promotion of angiogenesis and fibroblast function. Theranostics *8*, 169–184.

12. van de Ven, R.A.H., Santos, D., and Haigis, M.C. (2017). Mitochondrial Sirtuins and Molecular Mechanisms of Aging. Trends Mol. Med. *23*, 320–331.
13. Jeelani, R., Khan, S.N., Shaeib, F., Kohan-Ghadr, H.R., Aldhaheri, S.R., Najafi, T., Thakur, M., Morris, R., and Abu-Soud, H.M. (2017). Cyclophosphamide and acrolein induced oxidative stress leading to deterioration of metaphase II mouse oocyte quality. Free Radic. Biol. Med. *110*, 11–18.
14. Di Emidio, G., Falone, S., Vitti, M., D'Alessandro, A.M., Vento, M., Di Pietro, C., Amicarelli, F., and Tatone, C. (2014). SIRT1 signalling protects mouse oocytes against oxidative stress and is deregulated during aging. Hum. Reprod. *29*, 2006–2017.
15. Lim, J., and Luderer, U. (2011). Oxidative damage increases and antioxidant gene expression decreases with aging in the mouse ovary. Biol. Reprod. *84*, 775–782.
16. Tsai-Turton, M., Luong, B.T., Tan, Y., and Luderer, U. (2007). Cyclophosphamide-induced apoptosis in COV434 human granulosa cells involves oxidative stress and glutathione depletion. Toxicol. Sci. *98*, 216–230.
17. Tatone, C., Di Emidio, G., Barbonetti, A., Carta, G., Luciano, A.M., Falone, S., and Amicarelli, F. (2018). Sirtuins in gamete biology and reproductive physiology: emerging roles and therapeutic potential in female and male infertility. Hum. Reprod. Update *24*, 267–289.
18. Min, Z., Gao, J., and Yu, Y. (2019). The Roles of Mitochondrial SIRT4 in Cellular Metabolism. Front. Endocrinol. (Lausanne) *9*, 783.
19. Wood, J.G., Schwer, B., Wickremesinghe, P.C., Hartnett, D.A., Burhenn, L., Garcia, M., Li, M., Verdin, E., and Helfand, S.L. (2018). Sirt4 is a mitochondrial regulator of metabolism and lifespan in *Drosophila melanogaster*. Proc. Natl. Acad. Sci. USA *115*, 1564–1569.
20. Zeng, J., Jiang, M., Wu, X., Diao, F., Qiu, D., Hou, X., Wang, H., Li, L., Li, C., Ge, J., et al. (2018). SIRT4 is essential for metabolic control and meiotic structure during mouse oocyte maturation. Aging Cell *17*, e12789.
21. Ho, L., Titus, A.S., Banerjee, K.K., George, S., Lin, W., Deota, S., Saha, A.K., Nakamura, K., Gut, P., Verdin, E., and Kolthur-Seetharam, U. (2013). SIRT4 regulates ATP homeostasis and mediates a retrograde signaling via AMPK. Aging (Albany NY) *5*, 835–849.
22. Lang, A., Anand, R., Altinoluk-Hambüchen, S., Ezzahoini, H., Stefanski, A., Iram, A., Bergmann, L., Urbach, J., Böhler, P., Hänsel, J., et al. (2017). SIRT4 interacts with OPA1 and regulates mitochondrial quality control and mitophagy. Aging (Albany NY) *9*, 2163–2189.
23. Martins-de-Souza, D., Harris, L.W., Guest, P.C., and Bahn, S. (2011). The role of energy metabolism dysfunction and oxidative stress in schizophrenia revealed by proteomics. Antioxid. Redox Signal. *15*, 2067–2079.
24. Ding, C., Zou, Q., Wang, F., Wu, H., Chen, R., Lv, J., Ling, M., Sun, J., Wang, W., Li, H., and Huang, B. (2018). Human amniotic mesenchymal stem cells improve ovarian function in natural aging through secreting hepatocyte growth factor and epidermal growth factor. Stem Cell Res. Ther. *9*, 55.
25. Zhang, Q., Bu, S., Sun, J., Xu, M., Yao, X., He, K., and Lai, D. (2017). Paracrine effects of human amniotic epithelial cells protect against chemotherapy-induced ovarian damage. Stem Cell Res. Ther. *8*, 270.
26. Zhang, Z., Yang, J., Yan, W., Li, Y., Shen, Z., and Asahara, T. (2016). Pretreatment of Cardiac Stem Cells With Exosomes Derived From Mesenchymal Stem Cells Enhances Myocardial Repair. J. Am. Heart Assoc. *5*, e002856.
27. Pegtel, D.M., Cosmopoulos, K., Thorley-Lawson, D.A., van Eijndhoven, M.A., Hopmans, E.S., Lindenberg, J.L., de Gruijl, T.D., Würdinger, T., and Middeldorp, J.M. (2010). Functional delivery of viral miRNAs via exosomes. Proc. Natl. Acad. Sci. USA *107*, 6328–6333.
28. Desrochers, L.M., Bordeleau, F., Reinhart-King, C.A., Cerione, R.A., and Antonyak, M.A. (2016). Microvesicles provide a mechanism for intercellular communication by embryonic stem cells during embryo implantation. Nat. Commun. *7*, 11958.
29. Santonocito, M., Vento, M., Guglielmino, M.R., Battaglia, R., Wahlgren, J., Ragusa, M., Barbagallo, D., Borzì, P., Rizzari, S., Maugeri, M., et al. (2014). Molecular characterization of exosomes and their microRNA cargo in human follicular fluid: bioinformatic analysis reveals that exosomal microRNAs control pathways involved in follicular maturation. Fertil. Steril. *102*, 1751–17561.e1.
30. Xu, D.Q., Wang, Z., Wang, C.Y., Zhang, D.Y., Wan, H.D., Zhao, Z.L., Gu, J., Zhang, Y.X., Li, Z.G., Man, K.Y., et al. (2016). PAQR3 controls autophagy by integrating AMPK signaling to enhance ATG14L-associated PI3K activity. EMBO J. *35*, 496–514.
31. Tao, R., Gong, J., Luo, X., Zang, M., Guo, W., Wen, R., and Luo, Z. (2010). AMPK exerts dual regulatory effects on the PI3K pathway. J. Mol. Signal. *5*, 1.
32. Carracedo, A., and Pandolfi, P.P. (2008). The PTEN-PI3K pathway: of feedbacks and cross-talks. Oncogene *27*, 5527–5541.
33. Liu, M., Wang, Z., Ren, M., Yang, X., Liu, B., Qi, H., Yu, M., Song, S., Chen, S., Liu, L., et al. (2019). SIRT4 regulates PTEN stability through IDE in response to cellular stresses. FASEB J. *33*, 5535–5547.
34. Tang, H., Lee, M., Sharpe, O., Salamone, L., Noonan, E.J., Hoang, C.D., Levine, S., Robinson, W.H., and Shrager, J.B. (2012). Oxidative stress-responsive microRNA-320 regulates glycolysis in diverse biological systems. FASEB J. *26*, 4710–4721.
35. Ren, X.P., Wu, J., Wang, X., Sartor, M.A., Jones, K., Qian, J., Nicolaou, P., Pritchard, T.J., and Fan, G.C. (2009). MicroRNA-320 is involved in the regulation of cardiac ischemia/reperfusion injury by targeting heat-shock protein 20. Circulation *119*, 2357–2366.
36. Feng, R., Sang, Q., Zhu, Y., Fu, W., Liu, M., Xu, Y., Shi, H., Xu, Y., Qu, R., Chai, R., et al. (2015). MiRNA-320 in the human follicular fluid is associated with embryo quality in vivo and affects mouse embryonic development in vitro. Sci. Rep. *5*, 8689.
37. Yin, M., Wang, X., Yao, G., Lü, M., Liang, M., Sun, Y., and Sun, F. (2014). Transactivation of micrornA-320 by microRNA-383 regulates granulosa cell functions by targeting E2F1 and SF-1 proteins. J. Biol. Chem. *289*, 18239–18257.